

Article

A Chemical Safety Assessment of Lyocell-Based Activated Carbon Fiber with a High Surface Area through the Evaluation of HCl Gas Adsorption and Electrochemical Properties

Jong Gu Kim ¹  and Byong Chol Bai ^{2,*} 

¹ National Research Safety Headquarters, Korea Research Institute of Bioscience and Biotechnology, Cheongju 28116, Republic of Korea; kim@kribb.re.kr

² Division of Energy Engineering, Daejin University, Pocheon 11159, Republic of Korea

* Correspondence: baibc0820@daejin.ac.kr

Abstract: This study investigates lyocell-based activated carbon fibers (ACFs) for their suitability in adsorbing and electrochemically detecting toxic HCl gas. ACFs were prepared via steam activation, varying temperature (800–900 °C) and time (40–240 min) to assess their adsorption and sensing capabilities. The adjustment of activation temperature and reaction time aimed to regulate the uniformity of the pore structure and pore size of the active reaction area, as well as the number of reaction sites in the ACFs. Optimal ACFs were achieved at 900 °C for 50 min, exhibiting the highest specific surface area (1403 m²/g) and total pore volume (0.66 cm³/g). Longer reaction times resulted in pore formation and disorder, reducing mechanical strength. The ACFs prepared under optimal conditions demonstrated a rapid increase in resistance during sensor measurement, indicating a significant sensitivity to HCl gas. These findings suggest the potential of ACFs for efficient HCl gas adsorption (1626.20 mg/g) and highlight the importance of activation parameters in tailoring their properties for practical applications.

Keywords: chemical safety assessment; activated carbon fiber; HCl gas; adsorption; gas sensing



Citation: Kim, J.G.; Bai, B.C. A Chemical Safety Assessment of Lyocell-Based Activated Carbon Fiber with a High Surface Area through the Evaluation of HCl Gas Adsorption and Electrochemical Properties. *Separations* **2024**, *11*, 79. <https://doi.org/10.3390/separations11030079>

Academic Editor: Xinhua Qi

Received: 23 January 2024

Revised: 22 February 2024

Accepted: 28 February 2024

Published: 2 March 2024



Copyright: © 2024 by the authors. Licensee MDPI, Basel, Switzerland. This article is an open access article distributed under the terms and conditions of the Creative Commons Attribution (CC BY) license (<https://creativecommons.org/licenses/by/4.0/>).

1. Introduction

The intricate connection between the sustained well-being of living organisms and their surrounding environment has been a foundational principle in ecological discourse [1–3]. Regrettably, there has been a significant surge in environmental degradation, particularly attributed to the pervasive impact of air pollution in recent decades [4–7]. Air pollution (comprising a broad spectrum of pollutants such as hazardous gases, particulate matter, and noxious fumes) poses a multifaceted threat. Among these pollutants, hazardous gases stand out as particularly menacing due to their potential to trigger various diseases, carcinogenesis, and even fatalities [8,9]. Of significant concern is hydrochloride (HCl), originating commonly from chemical, metallurgical, pharmaceutical industries, or waste incineration, which emerges as one of the most perilous hazardous gases.

When HCl gas is released, it can induce acidification in both soil and water, presenting substantial risks to plant life up to and including fatality. The detrimental effects extend beyond vegetation to impact humans and animals, and can lead to skin damage, irritation, and mucosal tissue harm in the eyes and respiratory passages [10,11]. Consequently, there is a pressing need for the development of highly sensitive HCl sensors. These sensors play a crucial role in the early detection and continuous monitoring of HCl leaks, allowing for proactive measures to counteract potential accidental threats [12]. This underscores the significance of advancing sensor technologies for the preservation of both environmental and human health. Given the multifaceted dangers posed by HCl, the development of efficient sensors is not just a technological imperative but also a vital step in safeguarding ecosystems and public well-being. By enhancing our ability to promptly detect and respond

to HCl leaks, these sensors contribute to a proactive approach in mitigating the harmful impacts on ecosystems, human health, and overall environmental sustainability [13]. Therefore, ongoing advancements in sensor technology are pivotal for maintaining a healthy balance between technological progress and environmental protection.

As the demand for improved sensor capabilities grows, there is a concurrent surge in research exploring various adsorbents for sensor applications. Frequently, zeolites, metal-organic frameworks (MOF), and porous carbon materials serve as effective adsorbents for a variety of pollutants. Among these, activated carbon (AC) and activated carbon fiber (ACF) stand out as commonly utilized porous carbon materials [14–16], and are being investigated for their efficacy in capturing and detecting HCl and other pollutants [17]. AC is extensively employed for eliminating harmful substances and gases from industrial gas streams. The specific surface area of these materials is a critical parameter and is significantly influenced by the chosen activation method. By carefully optimizing synthetic conditions, it is possible to achieve surface areas ranging from 500 to 1500 m²/g, with a micropore yield reaching up to 70%. This results in the production of highly adsorbent AC [18,19]. Despite their effectiveness, these materials have limitations in terms of recyclability, and the breakthrough point—indicating gas adsorption saturation—is relatively short. Notably, these challenges are closely linked to particle morphology [20,21]. Addressing these challenges is pivotal for the development of advanced adsorbents, aiming to enhance both recyclability and breakthrough points. As research progresses, efforts to optimize particle morphology and fine-tune synthetic conditions will play a crucial role in improving the overall performance and sustainability of these porous carbon materials [22]. Striking a balance between high adsorption capacity and enhanced recyclability is essential for the continuous advancement of adsorbent technologies in addressing environmental pollution.

In contrast to AC, ACF boasts a fiber surface with relatively uniform micropores, leading to a faster gas adsorption rate compared to AC. The distinct advantage lies in the ease of separation from adsorbates, resulting in high recyclability [23]. Furthermore, the unique pore structure of ACF contributes to its exceptional physisorption and chemisorption capabilities. Modification with functional groups to enhance sorption properties is easily achievable. Leveraging these attributes, ACF has found applications as a material for adsorption filters targeting the removal of harmful gases [24,25]. Beyond filtration, ACFs serve as exceptional porous electrode materials due to their outstanding electrical conductivity. Moreover, they have garnered attention as materials for gas sensors capable of detecting harmful gases. This is particularly notable for their operational stability at high temperatures, a characteristic that sets them apart from conventional catalytic combustion or semiconductor gas sensors [26,27]. Consequently, the study and improvement of ACFs, along with a comprehensive analysis of their properties, has emerged as a pivotal endeavor for the ongoing development of advanced sorbents and sensing materials. Understanding and enhancing the unique features of ACFs plays a crucial role in shaping the landscape of materials used for gas adsorption, filtration, and sensing applications, contributing to advancements in environmental and industrial technologies [28]. Compared to materials commonly used for detecting HCl gas, ACFs offer several distinguishing features. Firstly, their fiber surface with uniform micropores enables a faster adsorption rate, enhancing their efficiency in capturing HCl molecules effectively. Additionally, the unique pore structure of ACFs and their ability to modify them with functional groups allow for tailored sorption properties, improving their selectivity and sensitivity towards HCl detection. Furthermore, ACFs' exceptional electrical conductivity and operational stability at high temperatures set them apart from conventional materials typically used for gas detection purposes. These characteristics make ACFs a promising candidate for HCl detection applications, offering superior performance and versatility compared to traditional sensing materials. This study was dedicated to assessing the suitability of the lyocell-based activated carbon fibers (ACFs) for the adsorption and electrochemical detection of toxic HCl gas. The alterations in microtextural properties were induced by the pyrolysis of lyocell fibers followed by steam activation. The primary focus was on investigating the impact of activation conditions on

the performance of the ACFs. In essence, steam activation was employed to deliberately vary and optimize the specific surface area and pore characteristics of the carbon materials. The textural properties, encompassing factors such as specific surface area and pore structure, were systematically evaluated with the aim of understanding their potential application in the adsorption of harmful gases. By fine-tuning the activation conditions, the study aimed to elucidate the correlation between microtextural variations in the lyocell-based ACFs and their effectiveness in adsorbing and detecting HCl gas. This research contributes to the ongoing exploration of advanced materials with tailored properties for applications in environmental and industrial gas management.

2. Materials and Methods

2.1. Preparation of ACF and Pore Characteristics

In this study, we optimized the conditions for preparing ACFs from lyocell fiber (Kolon Industries, Inc., Seoul, Republic of Korea). Our primary emphasis was on achieving desirable specific surface area and yield, with a particular interest in investigating various steam activation conditions within the temperature range of 800–900 °C. Before subjecting the lyocell fiber to steam activation, we employed di-ammonium-hydrogen phosphate (DAHP), obtained from Sigma-Aldrich Co., St. Louis, MO, USA, as a flame-retardant agent [10]. The choice of DAHP was driven by its potential to enhance the yield of lyocell fiber, specifically for carbon fiber production. In our initial treatment step, 10 g of raw lyocell fiber underwent immersion in 100 mL of 7 wt% DAHP solutions for a duration of 5 h at 60 °C. After the reaction, the solution was removed by filtration, and the samples were subsequently dried overnight at 70 °C under vacuum. Before carbonization, the lyocell fibers underwent stabilization at 300 °C for 30 min in the air gas. These conditions were determined based on optimal chemical treatment conditions established in our prior work [6]. The stabilized lyocell fiber, now prepared for carbon fiber production, was positioned in an alumina boat within a reactor. The sample underwent heating at temperatures of 1000 °C for 1 h under a nitrogen gas (N₂, purity: 99.999%) atmosphere. The heating rate employed was 10 °C/min, and a N₂ gas feed rate of 100 mL/min was maintained throughout the process. This meticulous process aimed to successfully convert lyocell fiber into activated carbon fiber, with specific attention given to achieving optimal surface area and yield under the specified steam activation conditions.

In the steam activation process, 1 g of carbon fibers were placed in an alumina boat within a reactor. Then, the temperature underwent a gradual increase of 5 °C/min within an N₂ gas atmosphere to reach target temperature. Upon reaching the desired activation temperature range of 800, 850, and 900 °C, water was introduced at a rate of 10 mL/min, generating steam to react with the carbon fibers. Each sample was subsequently maintained at the designated reaction temperature for 1 h to ensure optimal activation. After the reaction, the samples were dried for 24 h in a 120 °C oven. Our investigation delved into the alterations in pore structure resulting from varying activation conditions. Additionally, we explored changes in pore structure by manipulating activation reaction time while keeping the temperature constant, treating both process temperature and reaction time as variables. To determine the micropore structures of the ACFs, we utilized Brunauer–Emmett–Teller (BET) specific surface area analysis (Micromeritics Instrument Co., ASAP2020, Norcross, GA, USA). This analysis allowed us to understand the micropore structures of ACFs and accurately determine their porosity. Furthermore, the deliberate variation of activation parameters aimed to uncover the optimal conditions for enhancing both the specific surface area and pore structure of ACFs, which is critical for maximizing their performance in various applications. Overall, the comprehensive analysis of adsorption data obtained across a relative pressure (P/P_0) range spanning from 10^{-5} to 1 and conducted at 77 K provides valuable insights into the evolving micropore structures of ACFs under different activation conditions. This analysis allowed us to obtain N₂ adsorption isotherm results, elucidating the behavior of adsorption properties within the activated carbon fibers. The determination of micropore surface area employs the t-plot method, which utilizes the

carbon black STSA equation. This method facilitates the calculation of the external surface area, encompassing medium and large pores, by analyzing the slope in each corresponding range. Subsequently, the surface area of micropores was determined by subtracting the external specific surface area from the BET-specific surface area. Micropore volume was ascertained through the interception of the t-plot line. However, the t-plot method, while commonly used for interpreting pore structures, possesses inherent limitations. To address these limitations, we employed the nonlocal density functional theory (NLDFT) method. NLDFT offers a more comprehensive approach to characterizing microporous materials, providing enhanced accuracy and reliability in pore size distribution (PSD) analysis. By leveraging NLDFT alongside the t-plot method, we aimed to overcome the shortcomings associated with the sole reliance on traditional techniques, thereby ensuring a more robust and insightful investigation into the micropore structures of the materials under study. The total pore volume (V_t) was computed utilizing NLDFT. To derive the average pore width, a cylindrical morphology of pores was assumed based on the BET surface area (S_{BET}) and pore volume (V_t), with the formula $d = 4V_t/S_{BET}$.

2.2. Mechanical Strength

To assess mechanical strength (a key determinant of the durability of ACFs), we conducted tensile strength measurements using a fiber tensile tester (SHIMADZU, AG-X, Japan). The ACF samples of varying activation conditions were fashioned into tensile specimens with a length of 25 mm. In the measurement process, a single strand of the collected ACF was carefully positioned on the specimen frame and affixed with epoxy resin to ensure the fiber was taut. For the tensile tests, a minimum of 10 specimens per ACF obtained under each activation condition were meticulously prepared. Each experiment was replicated 10 times, and the average results were computed. Additionally, the tensile modulus of elasticity was determined by analyzing the slope of the obtained results. These mechanical strength evaluations provide crucial insights into the robustness and resilience of the ACFs under different activation conditions, contributing valuable data to the understanding of their potential applications in real-world scenarios.

2.3. Electrochemical HCl Gas Sensing

For the assessment of HCl gas sensing properties, a single strand of the collected ACF was selected, and both ends were affixed to a glass plate using a silver paste, following the same methodology outlined in Section 2.2. Sensor electrodes were then fashioned by attaching a 50 mm silver wire to both sides of the ACFs. The electrode, complete with the silver wire, was positioned at the center of the reactor, and the gas-sensing properties were evaluated at room temperature. To measure the gas sensing properties, the concentration was controlled based on a 20 ppm concentration of HCl gas (used purity 99.999% N₂ gas as balance gas, Rigas Co., Daejeon, Republic of Korea). Throughout the experiment, a constant gas flow rate of 500 sccm was maintained using a mass flow controller (MFC). The resistance change of the electrode in response to HCl gas exposure was monitored and measured using a system electrometer (Keithley 6514, Solon, OH, USA) [18]. This experimental setup allowed for a systematic evaluation of the ACF's responsiveness to varying concentrations of HCl gas, providing valuable insights into its potential utility as a gas sensor.

2.4. Analysis of HCl Adsorption

To comprehend the HCl gas adsorption properties of different activated carbon fibers (ACFs), the extent of HCl adsorption per gram of ACF used in the analysis was assessed employing an HCl gas detector (Wandi Technology Co., Ltd., FIX800-HCl, Hangzhou, China). The adsorption degree of ACFs was determined based on the input time of 20 ppm HCl gas. This information was calculated using the following equations:

$$V_{eff} = Q \cdot t_{total} \quad (1)$$

$$m_{total} = \frac{C_0 V_{eff}}{1000} \tag{2}$$

$$q_{total} = \frac{Q}{1000} \int_{t=0}^{t=t_{total}} C_{ad} dt \tag{3}$$

$$R_{total} = \frac{q_{total}}{m_{total}} \times 100 \tag{4}$$

Equation (1) gives the total input amount of HCl gas, V_{eff} (L). Q (L/min) is the gas flow, and t_{total} (min) is the gas input time. Equation (2) is an expression to calculate the amount of HCl, m_{total} (mg/g), in the total gas input per gram of ACF. C_0 (mg/L) is the concentration of HCl. Equation (3) is an expression to calculate the amount of HCl gas adsorbed on the ACF per gram of ACF, q_{total} (mg/g), which was calculated using the integral formula for the amount of adsorbed gas (C_{ad}) according to gas input time (t , min). In Equation (4), R_{total} (%) is the rate of adsorption of HCl gas [11]. In addition to the equations above, the breakthrough point and the breakthrough time (t_b) were determined as follows: in the breakthrough curve, $C/C_0 = 0.05$ was determined as the breakthrough point, and the time was determined as the breakthrough time. In addition, when $C/C_0 = 0.95$ was reached, it was judged that the adsorption of the ACF was saturated, and the time was determined as the saturation time (t_s). The adsorption properties of ACFs are highly related to the pore structure created in the activation process. Therefore, the adsorption properties were evaluated after selecting the sample with the highest specific surface area for each temperature. To ensure the reproducibility and reliability of our findings, we carried out three repetitive evaluations of HCl adsorption characteristics using a consistent methodology. These repeated assessments were intended to confirm the consistency and robustness of our experimental approach in characterizing HCl adsorption properties under identical conditions.

3. Results and Discussion

3.1. Pore Structure of ACFs with Steam Activation Temperature and Time

As shown in Figure 1 and Table 1, the specific surface area of the ACFs increased as the activation temperature and the activation time increased. The activation condition that gave the highest specific surface area was the activation temperature of 900 °C and the reaction time of 50 min. At that condition, the specific surface area was 1403 m²/cm. Also, the sample yield decreased at every activation condition as the activation temperature increased and the reaction time increased. For the samples prepared below 900 °C (the highest temperature used), there was an increase in the specific surface area with an increase in time. However, when the reaction time exceeded 50 min, a sudden decrease was noted, attributed to the phenomena of the expansion and collapse of pores [29,30]. Under the reaction conditions of 900 °C for 60 min, a decrease in specific surface area to 1044 m²/g and micropore volume to 0.41 cm³/g was observed. These results are believed to be attributed to the collapse of the pore structure due to excessive activation reaction.

Table 1. Specific surface area and microporosity of ACFs prepared under various steam activation conditions.

| T (°C) | t (min) | Yield (%) | S_{BET} (m ² /g) | V_{micro} (cm ³ /g) | V_{total} (cm ³ /g) |
|-------------|--------------|--------------|----------------------------------|-------------------------------------|-------------------------------------|
| 800 | 120 | 54.15 | 949 | 0.36 | 0.41 |
| | 180 | 48.33 | 1021 | 0.39 | 0.44 |
| | 240 | 40.02 | 1113 | 0.44 | 0.50 |
| 850 | 60 | 45.98 | 1066 | 0.42 | 0.46 |
| | 80 | 39.20 | 1119 | 0.44 | 0.52 |
| | 100 | 34.69 | 1204 | 0.48 | 0.56 |

Table 1. Cont.

| T (°C) | t (min) | Yield (%) | S_{BET} (m ² /g) | V_{micro} (cm ³ /g) | V_{total} (cm ³ /g) |
|-------------|--------------|--------------|----------------------------------|-------------------------------------|-------------------------------------|
| 900 | 40 | 42.44 | 869 | 0.34 | 0.38 |
| | 50 | 36.66 | 1403 | 0.57 | 0.66 |
| | 60 | 30.11 | 1044 | 0.41 | 0.48 |

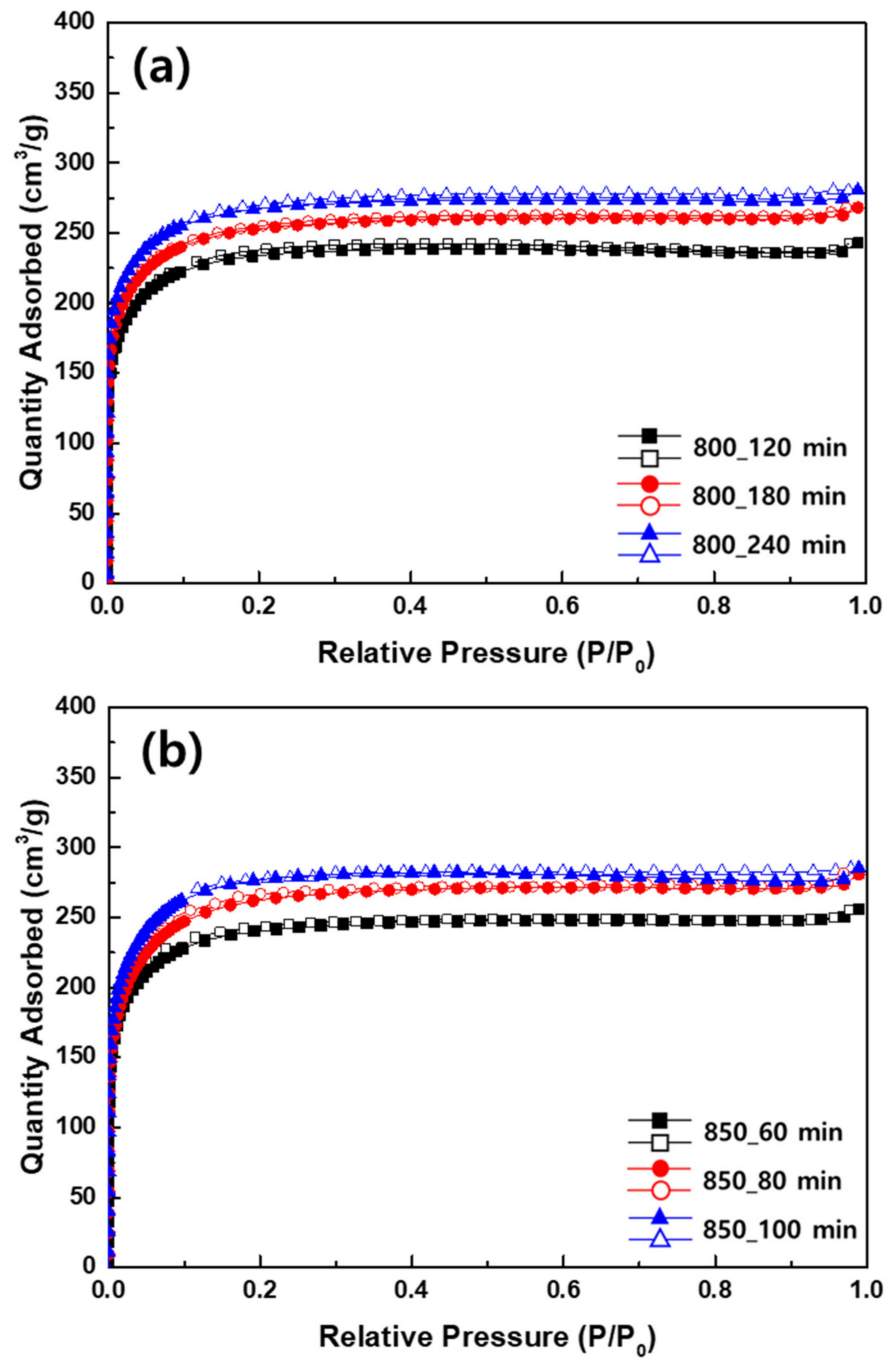


Figure 1. Cont.

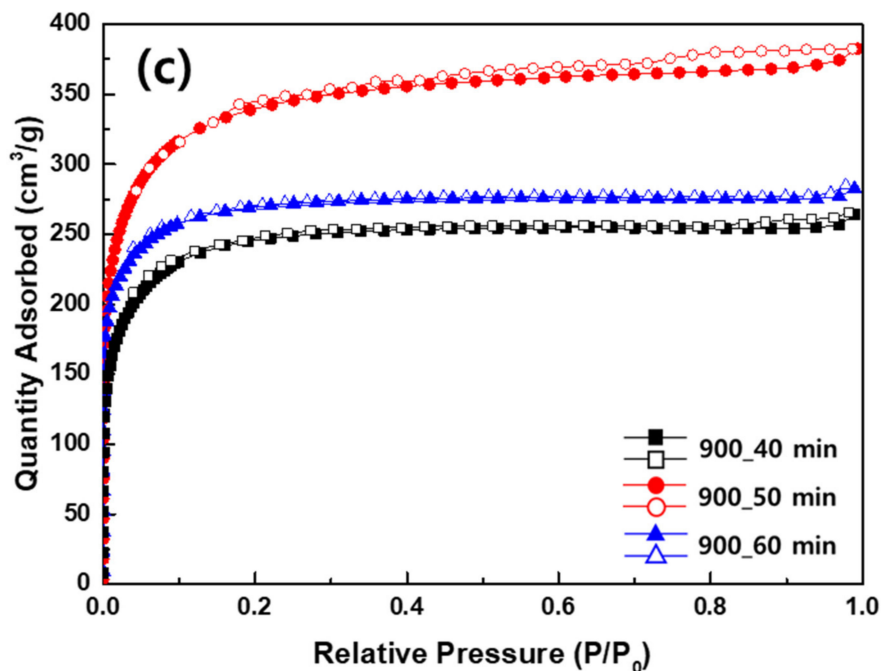


Figure 1. N₂ isotherms of ACFs prepared under various steam activation conditions: (a) reaction temperature: 800 °C, reaction time: 120–240 min; (b) reaction temperature: 850 °C, reaction time: 60–100 min; and (c) reaction temperature: 900 °C, reaction time: 40–60 min.

The PSD data of the ACFs underwent comparative analysis, with the results depicted in Figure 2. The samples demonstrated the development of both micropores and mesopores within the range of 0.5–20 nm. Micropores, characterized by peak pore widths of 0.5 to 2 nm, along with mesopores exhibiting a prominent peak at 5 to 10 nm, significantly contribute to gas molecule adsorption, thereby playing a crucial role in applications involving harmful gases. It was observed that as the activation temperature increased, there was a notable development in the pore structure. However, under the activation conditions of 900 °C for 60 min, excessive activation reactions led to the overall collapse of the pore structure.

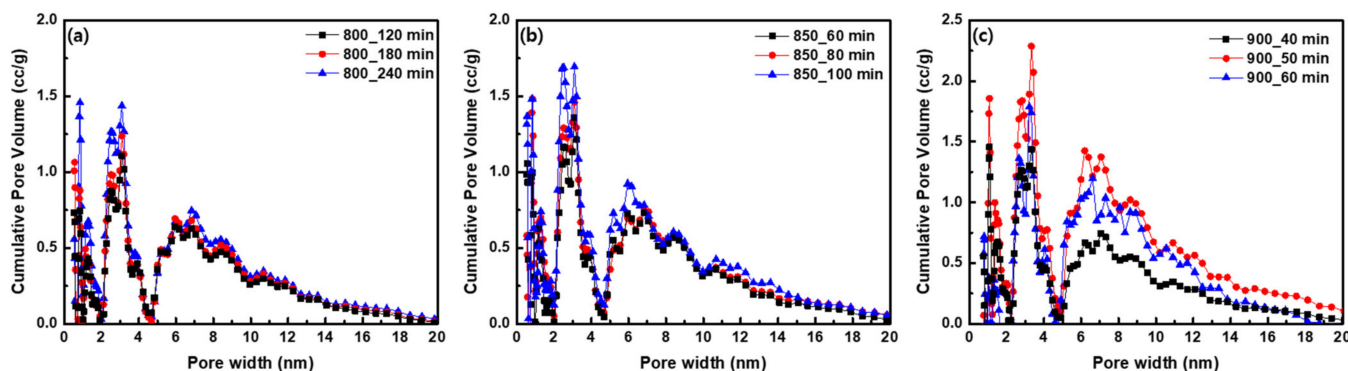


Figure 2. Pore size distribution of ACFs prepared under various steam activation conditions: (a) reaction temperature: 800 °C, reaction time: 120–240 min; (b) reaction temperature: 850 °C, reaction time: 60–100 min; and (c) reaction temperature: 900 °C, reaction time: 40–60 min.

3.2. Analysis of Mechanical Strengths of ACFs

An analysis was conducted to measure the mechanical strength of ACFs, and the results are presented in Figure 3. As depicted in Figure 3, the tensile strength and tensile modulus of ACFs decreased with increasing steam activation time and activation temperature. The mechanical strength of ACFs decreased because pores were formed as the carbon framework decomposed into CO, CO₂, and H₂O. With an increase in reaction time, the

structure of the ACFs became more disordered. Therefore, both the tensile strength and elastic modulus tended to decrease. During steam activation, higher temperatures result in the reaction of more activation sites as well as an increase in the reaction rate, causing the structure to collapse faster and pores to form [31].

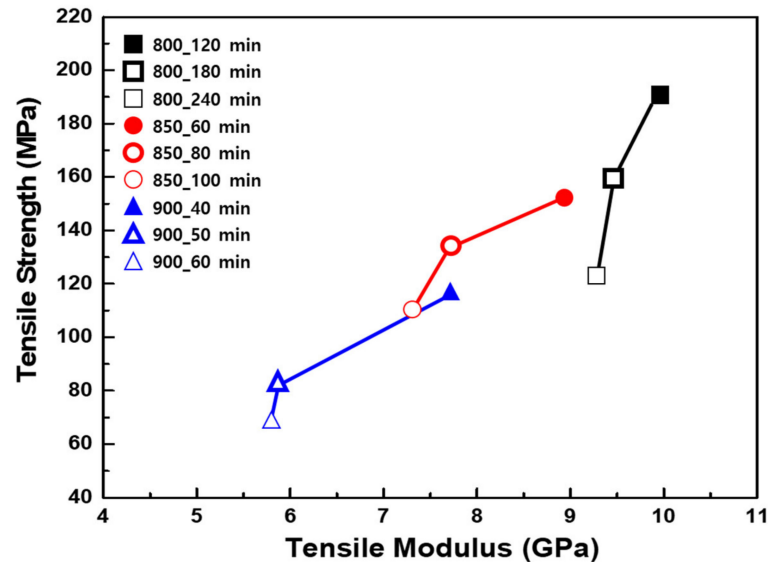


Figure 3. Tensile strength versus tensile modulus of ACFs prepared under different steam-activation conditions.

3.3. Analysis of Resistive Response of ACFs

The resistive response of activated carbon fiber was measured according to the degree of HCl gas adsorption, and is shown in Figure 4. The y-axis is the rate of change in the resistance ($S\%$) during the flow of the target gas compared to the initial resistance, that is, $(R - R_0)/R_0 \times 100\%$, where R is the measured resistance and R_0 is the initial resistance. As shown in Figure 4, the rate of change in the resistance with respect to the steam activation time increased linearly, probably because the specific surface area increased and the micropore structure developed with an increase in activation time, as shown by the BET results. Furthermore, as the pore structure developed the adsorption of HCl gas increased, resulting in a change in resistance. Therefore, longer activation of the sample resulted in greater change in resistance. In the case of the sample prepared at 900 °C for 50 min, which exhibited the highest specific surface area, the slope increased rapidly after sensor measurement commenced, indicating the most significant change in resistance. These results ultimately suggest that ACFs can serve as suitable materials for sensors, as they demonstrate significant changes in resistance in the presence of HCl gas.

The sensing mechanism can be explained as follows: HCl molecules are adsorbed into the pores of ACFs via van der Waals forces, and electron exchange occurs through semi-ionic interactions [31]. Generally, SnO_2 and carbon nanotubes are P-type semiconductors frequently used as gas-sensing materials. In the presence of such materials, oxidizing gases such as NO and CO_2 lose electrons, leading to an increase in the hole density in the valence band. Consequently, the Fermi level shifts closer to the valence band, resulting in a reduction in electrical resistance. In contrast, in the presence of reducing gases (HCl, SO_2 , NH_3 , etc.), electrons are obtained from the gas, causing a decrease in the density of holes. This shift makes the Fermi level move toward the conduction band, leading to an increase in electrical resistance [32,33]. In this study, the electrical resistance for all samples increased in the presence of the reducing HCl gas, as depicted in Figure 4. Therefore, these results suggest that ACFs function similarly to semiconductor-type gas sensors.

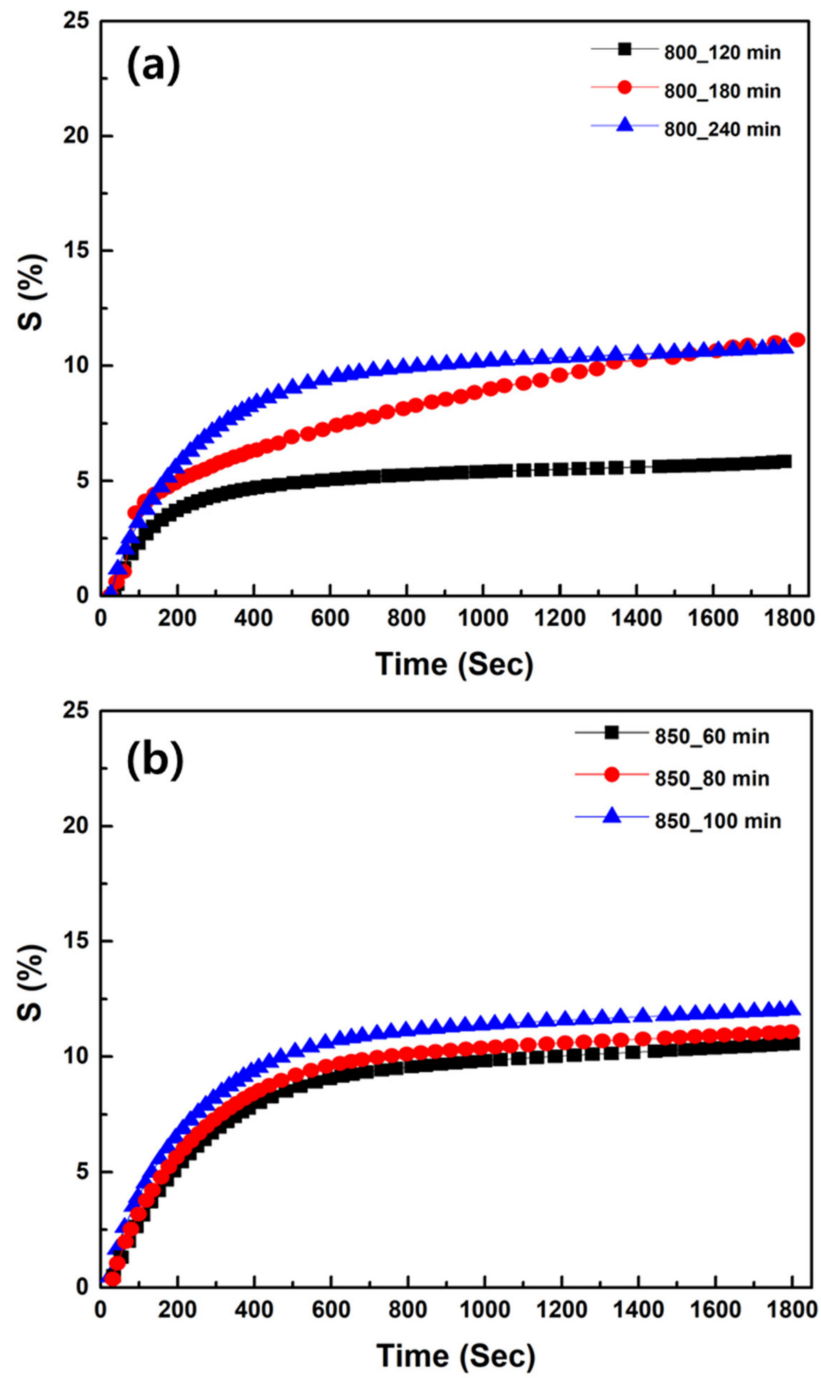


Figure 4. Cont.

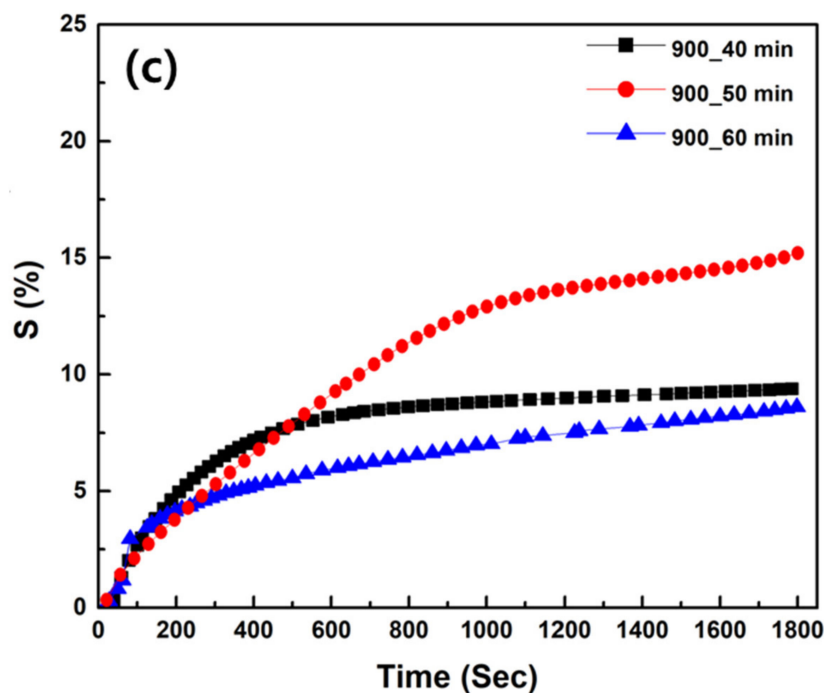


Figure 4. HCl gas resistive response property of ACFs fabricated under the following conditions: (a) reaction temperature: 800 °C, reaction time: 120–240 min; (b) reaction temperature: 850 °C, reaction time: 60–100 min; and (c) reaction temperature: 900 °C, reaction time: 40–60 min.

3.4. Analysis of the Adsorption of HCl Gas by ACFs

The HCl gas adsorption properties of the ACFs were determined using a HCl gas analyzer, and the results are shown in Figure 5 and Table 2. As shown in Figure 5a, adsorption analysis of HCl gas was performed on ACFs with the highest specific surface area at each temperature based on the activation conditions. As shown in Figure 5a, the ACFs prepared at 900 °C for 50 min, exhibiting the highest specific surface area among the prepared ACFs, displayed the most favorable HCl gas adsorption properties. This is likely attributed to the developed pore structure. Importantly, the highest amount of HCl gas adsorbed was 1626.20 mg/g. Additionally, the breakthrough time was 17.75 min, representing the longest duration of continuous gas adsorption among these samples. However, in terms of adsorption efficiency, the ACFs prepared at 850 °C for 100 min exhibited the highest performance, indicating that the mass transfer rate of HCl molecules was the greatest. As a result, with the increase in the specific surface area of the activated carbon fiber, the amount of HCl gas adsorbed and the breakthrough time also increased (800 °C, 240 min < 850 °C, 100 min < 900 °C, 50 min).

Additionally, the HCl gas adsorption capacity over three usage cycles was investigated and is presented in Figure 5b. In these experiments, ACFs prepared at 900 °C for 50 min, which had the highest specific surface area, were utilized. In brief, HCl gas was introduced into the sample tube, and the gas adsorption properties of the ACFs were measured. Following this, N₂ gas at room temperature was introduced to desorb the adsorbed gas. Subsequently, another adsorption cycle was conducted. The results for HCl gas adsorption are presented in Table 2. The amount of HCl gas adsorbed (q_{total}) decreased from 1626.20 to 1285.15 to 847.26 mg/g over the three measurements, indicating a total reduction of 52.1%. Consequently, the adsorption capacity of the ACFs declined with repeated use. This outcome may be attributed to the gases adsorbed through van der Waals interactions in the micropores of the ACFs not being adequately desorbed between cycles. It is noteworthy that the adsorption/desorption experiments were conducted at room temperature and pressure. Overall, the consistent trends in gas adsorption result from semi-ionic interaction and adsorption via van der Waals force in the micropores of the ACFs.

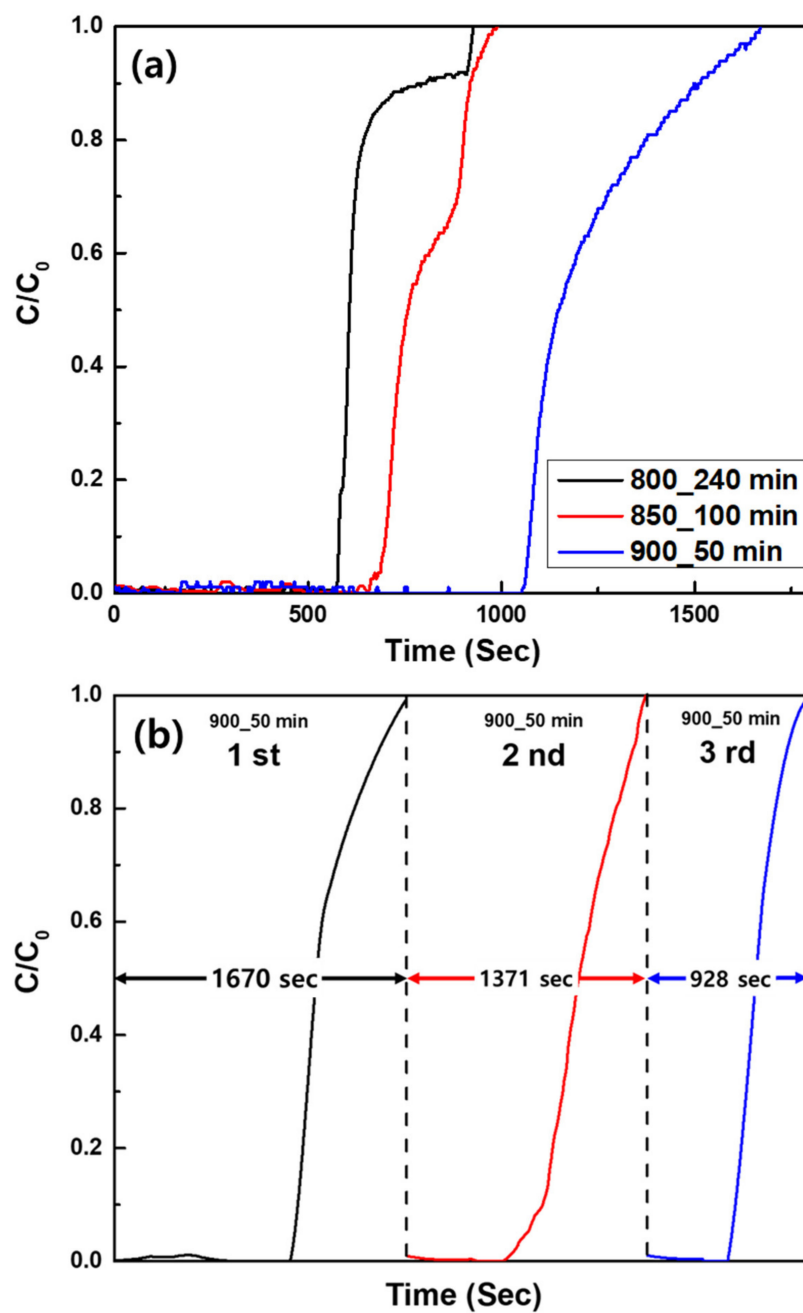


Figure 5. (a) HCl gas breakthrough curves and (b) recovery three times for the adsorption/desorption of 900_50 min sample.

Table 2. HCl gas adsorption properties by ACFs with maximum specific surface area for each activation condition.

| Sample | Superficial Velocity | Initial Concentration | Total Time | Breakthrough Time | Saturation Time | Effluent Volume | Total Amount Removed | Total Removal | Adsorption Capacity |
|-------------|----------------------|--------------------------|-----------------------------|----------------------------|----------------------------|-------------------------|------------------------------|---------------------------|------------------------------|
| | Q (L/min) | C ₀ (mg/L) | t _{total} (min) | t _{0.05} (min) | t _{0.95} (min) | V _{eff} (L) | m _{total} (mg/g) | R _{total} (%) | q _{total} (mg/g) |
| 800_240 min | 4000 | 20.03 | 15.42 | 9.65 | 15.32 | 61,680 | 1235.45 | 68.63 | 847.89 |
| 850_100 min | 4000 | 20.03 | 16.49 | 11.50 | 15.83 | 65,960 | 1321.18 | 80.09 | 1058.07 |

Table 2. Cont.

| Sample | Superficial Velocity | Initial Concentration | Total Time | Breakthrough Time | Saturation Time | Effluent Volume | Total Amount Removed | Total Removal | Adsorption Capacity |
|------------------|----------------------|-----------------------|----------------------|---------------------|---------------------|------------------|-----------------------|--------------------|-----------------------|
| | Q (L/min) | C_0 (mg/L) | t_{total} (min) | $t_{0.05}$ (min) | $t_{0.95}$ (min) | V_{eff} (L) | m_{total} (mg/g) | R_{total} (%) | q_{total} (mg/g) |
| 900_50 min (1st) | 4000 | 20.03 | 27.83 | 17.75 | 26.43 | 111,320 | 2229.74 | 72.93 | 1626.20 |
| 900_50 min (2nd) | 4000 | 20.03 | 22.85 | 11.51 | 22.11 | 91,400 | 1830.74 | 70.20 | 1285.15 |
| 900_50 min (3rd) | 4000 | 20.03 | 15.47 | 8.10 | 14.01 | 61,880 | 1239.46 | 68.36 | 847.26 |

4. Conclusions

In this study, we generated ACFs with elevated specific surface areas and uniform pores through the steam activation of lyocell-based carbon fibers at temperatures ranging from 800 to 900 °C. Significantly, the active reaction area was enhanced by manipulating the steam activation conditions, thereby maximizing the number of active sites. Furthermore, we conducted an analysis of the adsorption and sensing properties concerning hazardous HCl gas. Regarding the preparation of ACFs, the specific surface area of ACFs prepared at 900 °C increased with an extended reaction time until 50 min, after which it declined. This decrease is likely due to a rapid expansion and collapse of pores beyond this duration, predominantly influencing the formation of new pores through steam activation. Additionally, pores were formed as the carbon structure decomposed into CO, CO₂, and H₂O during steam activation, leading to a reduction in the mechanical strength of the ACFs. Upon analyzing the HCl gas resistive response properties of ACFs, the steam activation time and resistance change rate demonstrated a proportional relationship. Furthermore, with an increase in the specific surface area of the ACFs and the development of the micropore structure, excellent electrochemical gas sensing properties were achieved. Evaluating the HCl gas adsorption properties, the ACFs prepared at 900 °C for 50 min proved to be optimally adsorbent. This sample exhibited the longest breakthrough time and indicated the highest HCl adsorption capacity of 1626.20 mg/g. However, in terms of total removal efficiency, the result was lower at 72.93% compared with the ACFs prepared at 850 °C for 100 min, which showed a removal efficiency of 80.09%. This is attributed to an excessively high specific surface area, which may have prevented HCl gas molecules from penetrating deep into the micropores of the ACFs, thus affecting the overall removal efficiency. However, reusability diminished due to the high specific surface area and micropores. Therefore, for the development of sorbents for harmful gases, regeneration ability is crucial, and further research into the production of ACFs with high recyclability is warranted.

Author Contributions: Conceptualization and methodology, J.G.K. and B.C.B.; formal analysis, J.G.K.; data curation, J.G.K. and B.C.B.; writing—original draft, J.G.K.; writing—review and editing, B.C.B. All authors have read and agreed to the published version of the manuscript.

Funding: This research received no external funding.

Data Availability Statement: The data that support the findings of this study are available from the corresponding author upon reasonable request.

Conflicts of Interest: The authors declare no conflicts of interest.

References

1. Kelly, F.J.; Fussell, J.C. Air pollution and public health: Emerging hazards and improved understanding of risk. *Environ. Geochem. Health* **2015**, *37*, 631–649. [[CrossRef](#)]

2. Wee, J.H.; Bae, Y.; Ahn, H.; Choi, Y.O.; Jeong, E.; Yeo, S.Y. Fibrous and granular activated carbon mixed media for effective gas removal as a cabin air filter. *Carbon Lett.* **2022**, *32*, 1111–1118. [[CrossRef](#)]
3. Chen, Z.; Wang, J.N.; Ma, G.X.; Zhang, Y.S. China tackles the health effects of air pollution. *Lancet* **2013**, *382*, 1959–1960. [[CrossRef](#)]
4. Tabrizi, N.S.; Taleghani, M.S. Performance of CNT-CNP aerogel as an electrode in capacitive deionization system. *Carbon Lett.* **2023**, *33*, 1253–1263. [[CrossRef](#)]
5. Lelieveld, J.; Evans, J.S.; Fnais, M.; Giannadaki, D.; Pozzer, A. The contribution of outdoor air pollution sources to premature mortality on a global scale. *Nature* **2015**, *525*, 367–371. [[CrossRef](#)] [[PubMed](#)]
6. Brunekreef, B.; Holgate, S.T. Air pollution and health. *Lancet* **2002**, *360*, 1233–1242. [[CrossRef](#)] [[PubMed](#)]
7. Samet, J.M.; Gruskin, S. Air pollution, health, and human rights. *Lancet Resp. Med.* **2015**, *3*, 98–100. [[CrossRef](#)]
8. Natarajan, P.; Chandrababu, P.; Karmegam, P.M.; Madasamy, J.; Somasundaram, S. Tungsten-based activated carbon matrix for the catalytic oxidation of model volatile organic compounds (VOCs) and pharmaceutical VOCs from wastewater. *Carbon Lett.* **2023**, *33*, 1115–1132. [[CrossRef](#)]
9. Sivaranjane, R.; Kumar, P.S.; Rangasamy, G. A critical review on biochar for environmental applications. *Carbon Lett.* **2023**, *33*, 1407–1432. [[CrossRef](#)]
10. Bal, M.; Reddy, T.T.; Meikap, B.C. Removal of HCl gas from off gases using self-priming venturi scrubber. *J. Hazard. Mater.* **2019**, *364*, 406–418. [[CrossRef](#)]
11. Zhang, H.; Yu, S.; Shao, L.; He, P. Estimating source strengths of HCl and SO₂ emissions in the flue gas from waste incineration. *J. Environ. Sci.* **2019**, *75*, 370–377. [[CrossRef](#)]
12. Qiao, S.; Sampaolo, A.; Patimisco, P.; Spagnolo, V.; Ma, Y. Ultra-highly sensitive HCl-LITES sensor based on a low-frequency quartz tuning fork and a fiber-coupled multi-pass cell. *Photoacoustics* **2022**, *27*, 100381. [[CrossRef](#)]
13. Park, Y.K.; Oh, H.J.; Bae, J.H.; Lim, J.Y.; Lee, H.D.; Hong, S.I.; Son, H.S.; Kim, J.H.; Lim, S.J.; Lee, W. Colorimetric Textile Sensor for the Simultaneous Detection of NH₃ and HCl Gases. *Polymers* **2020**, *12*, 2595. [[CrossRef](#)]
14. Bai, B.C.; Im, J.S.; Lee, Y.S. Lyocell-based activated carbon fibers improved the adsorption of harmful gas properties when produced via dual-simultaneous treatments. *Carbon Lett.* **2017**, *23*, 69–73.
15. Dubinin, M.M. Microporous structures and absorption properties of carbonaceous adsorbents. *Carbon* **1983**, *21*, 359–366. [[CrossRef](#)]
16. Zhang, J.; Duan, Y.F.; Zhou, Q.; Zhu, C.; She, M.; Ding, W.K. Adsorptive removal of gas-phase mercury by oxygen non-thermal plasma modified activated carbon. *Chem. Eng. J.* **2016**, *294*, 281–289. [[CrossRef](#)]
17. Ravina, M.; Marotta, E.; Cerutti, A.; Zanetti, G.; Ruffino, B.; Panepinto, D.; Zanetti, M. Evaluation of Ca-Based sorbents for gaseous HCl emissions adsorption. *Sustainability* **2023**, *15*, 10882. [[CrossRef](#)]
18. Kim, M.J.; Lee, S.; Lee, K.M.; Jo, H.; Choi, S.S.; Lee, Y.S. Effect of CuO introduced on activated carbon fibers formed by electroless plating on the NO gas sensing. *J. Ind. Eng. Chem.* **2018**, *60*, 341–347. [[CrossRef](#)]
19. Han, J. Preparation of a highly sensitive graphene-based sensor to investigate the effect of exercise on electrolytes in sweat in hot and humid environment. *Carbon Lett.* **2023**, *33*, 1959–1966. [[CrossRef](#)]
20. Bai, B.C.; Kim, E.A.; Jeon, Y.P.; Lee, C.W.; In, S.J.; Lee, Y.S.; Im, J.S. Improved flame-retardant properties of lyocell fiber achieved by phosphorus compound. *Mater. Lett.* **2014**, *135*, 226–229. [[CrossRef](#)]
21. Kang, S.C.; Im, J.S.; Lee, Y.S. Improved sensitivity of an NO gas sensor by chemical activation of electrospun carbon fibers. *Carbon Lett.* **2011**, *12*, 21–25. [[CrossRef](#)]
22. Wang, H.; Wang, G.; Hu, L.; Ge, B.; Yu, X.; Deng, J. Porous polymer materials for CO₂ capture and electrocatalytic reduction. *Materials* **2023**, *16*, 1630. [[CrossRef](#)] [[PubMed](#)]
23. Saad, M.; Szymaszek, A.; Białas, A.; Samojeden, B.; Motak, M. SO₂ Poisoning and recovery of copper-based activated carbon catalysts for selective catalytic reduction of NO with NH₃ at low temperature. *Catalysts* **2020**, *10*, 1426. [[CrossRef](#)]
24. Park, M.S.; Lee, S.; Jung, M.J.; Kim, H.G.; Lee, Y.S. NO gas sensing ability of activated carbon fibers modified by an electron beam for improvement in the surface functional group. *Carbon Lett.* **2016**, *20*, 19–25. [[CrossRef](#)]
25. Aksu, Z.; Gönen, F. Biosorption of phenol by immobilized activated sludge in a continuous packed bed: Prediction of breakthrough curves. *Process Biochem.* **2004**, *39*, 599–613. [[CrossRef](#)]
26. Miller, D.R.; Akbar, S.A.; Morris, P.A. Nanoscale metal oxide-based heterojunctions for gas sensing. *A Rev. Sens. Act. B* **2014**, *204*, 250–272. [[CrossRef](#)]
27. Bai, J.; Huang, J.; Yu, Q.; Demir, M.; Akgul, E.; Altay, B.N.; Hu, X.; Wang, L. Fabrication of coconut shell-derived porous carbons for CO₂ adsorption application. *Front. Chem. Sci. Eng.* **2023**, *17*, 1122–1130. [[CrossRef](#)]
28. Hassan, M.F.; Sabri, M.A.; Fazal, H.; Hafeez, A.; Shezad, N.; Hussain, M. Recent trends in activated carbon fibers production from various precursors and applications—A comparative review. *J. Anal. Appl. Pyrolysis* **2020**, *145*, 104715. [[CrossRef](#)]
29. Kawabuchi, Y.; Oka, H.; Kawano, S.; Mochida, I.; Yoshizawa, N. The modification of pore size in activated carbon fibers by chemical vapor deposition and its effects on molecular sieve selectivity. *Carbon* **1998**, *36*, 377–382. [[CrossRef](#)]
30. Ko, T.H.; Chiranairadul, P.; Lu, C.K.; Lin, C.H. The effects of activation by carbon dioxide on the mechanical properties and structure of PAN-based activated carbon fibers. *Carbon* **1992**, *30*, 647–655. [[CrossRef](#)]
31. Bai, B.C.; Kim, E.A.; Lee, C.W.; Lee, Y.S.; Im, J.S. Effects of surface chemical properties of activated carbon fibers modified by liquid oxidation for CO₂ adsorption. *Appl. Surf. Sci.* **2015**, *353*, 158–164. [[CrossRef](#)]

32. Bannov, A.G.; Manakhov, A.M.; Shtansky, D.V. Plasma functionalization of multi-walled carbon nanotubes for ammonia gas sensors. *Materials* **2022**, *15*, 7262. [[CrossRef](#)]
33. Nag, A.; Alahi, M.E.E.; Mukhopadhyay, S.C.; Liu, Z. Multi-walled carbon nanotubes-based sensors for strain sensing applications. *Sensors* **2021**, *21*, 1261. [[CrossRef](#)]

Disclaimer/Publisher's Note: The statements, opinions and data contained in all publications are solely those of the individual author(s) and contributor(s) and not of MDPI and/or the editor(s). MDPI and/or the editor(s) disclaim responsibility for any injury to people or property resulting from any ideas, methods, instructions or products referred to in the content.